J Chapman et al.

The Dynamics of Magnetism in Fe-Cr Alloys with Cr Precipitation

The Dynamics of Magnetism in Fe-Cr Alloys with Cr Precipitation

Jacob B. J. Chapman,* Pui-Wai Ma, and Sergei L. Dudarev

UK Atomic Energy Authority, Culham Science Centre, Oxfordshire, OX14 3DB, United Kingdom

Magnetic plasma confinement is a key element of fusion tokamak power plant design, yet changes in magnetic properties of alloys and steels occurring under neutron irradiation are often overlooked. We perform a quantitative study exploring how irradiation-induced precipitation affects magnetic properties of Fe-Cr alloys. Magnetic properties are simulated over a broad temperature interval using spin dynamics, implemented using a Hamiltonian including longitudinal and transverse magnetic degrees of freedom. Simulations of alloys with nominal Cr concentrations in the range 0-25 at.%, and different microstructures, including disordered solid solutions and large Cr-rich precipitates, show that the Curie temperature T_C is always maximum when Cr solute concentration in the α phase is close to 5-6 at.%. The magnetic properties of Fe-9 at.%Cr alloys are found to vary by 10%, depending on the size of Cr clusters. We compute the magnetic susceptibility and time-displaced correlation functions of α' precipitates and (001) interfaces in Fe-Cr superlattices. A Cr interface disorders the Fe magnetic moments and acts as a nucleation site for the ferromagnetic-paramagnetic (FM-PM) transition with a lower effective T_C and enhanced susceptibility. Cr moments in disordered Fe-Cr alloys are highly non-collinear at all temperatures. Magnetic moments at interfacial Cr atoms remain correlated far above the Néel temperature, with correlations rapidly decreasing away from the interface. Spin dynamics simulations also offer insight into the time correlation functions and spin relaxation times in Fe-Cr alloys.

I. INTRODUCTION

Fe-Cr steels developed for fusion and fission applications are expected to sustain high irradiation doses approaching 10 to 20 displacements per atom (dpa) per full operation year[1,2]. Reduced Activation Ferritic Martensitic (RAFM) steels such as EUROFER-97 are the candidate materials for in-vessel applications due to their good strength and ductility, high fracture toughness, creep resistance and relatively low swelling under neutron irradiation[3,4]. Similar steels have been developed for applications in advanced fission reactors.

Iron and chromium are the main components of ferritic steels. They are both magnetic transition metals, and as a result Fe-Cr alloys exhibit rich structural and magnetic phase diagrams as a function of composition and temperature. At low temperatures, the alloys crystallize into a body-centred cubic (bcc) structure across the whole compositional range. Despite having similar lattice constants, where a^{Fe}=2.87Å and a^{Cr}=2.91Å, the phase diagram is composed of stable and metastable compositional domains. Between room temperature and 700K, a miscibility gap is observed starting from 5-10 at.%Cr and terminating at 90-95 at.%Cr. The precise boundaries remain contested[5–7]. Within the miscibility gap is the domain of spinodal decomposition. At temperatures above 1100K, iron and chromium are fully miscible.

The magnetic phases of Fe-Cr alloys are equally complex. The magnetic ground state of pure bcc Cr maintains an incommensurate spin density wave (SDW) below the Néel temperature $T_N^{\mathrm{exp}} \approx 310~K$. Spins of neighbouring atoms are aligned in an antiparallel configuration with magnitudes varying sinusoidally incommensurate with the lattice periodicity[8–10]. The introduction of isolated Fe elements into the Cr matrix reduces the antiferromagnetic (AFM) ordering by destabilising the

correlation between electron-hole pairs and making the SDW commensurate at 96-98 at.%Cr (α' phase). Between 81 and 84 at.%Cr, the Fe magnetic moments prevent long range AFM correlations, causing the moments to freeze into a spin glass[11]. For higher concentrations of Fe, the Fe-Cr system gains ferromagnetic (FM) ordering. The Curie temperature T_C is found to be maximised at $T_C^{\mathrm{exp}} \approx 1049$K for a dilute Cr concentration of 6 at.%[12]. This corresponds to the Fermi energy being at a minimum in the minority channel of the density of states, which favors the FM ordering of the iron magnetic moments[13].

Magnetic ordering also affects structural and mechanical properties of Fe-Cr alloys. For example, the magnetic free energy resulting from magnon and phonon excitations stabilize the FM bcc α phase of Fe in comparison with the HCP phase structure stabilized by the s and d orbital occupation alone[14,15]. Self-interstitial atom (SIA) defects in all the non-magnetic transition metals form $\langle 111 \rangle$ crowdion configurations[16,17]. On the other hand, SIAs in Fe and Fe-Cr alloys prefer a $\langle 110 \rangle$ dumbbell orientation with AFM-ordered spin moments in the core of the defect[18,19]. The softening of elastic constant C', observed near the Curie temperature in iron, is also caused by magnetic fluctuations[20,21].

RAFM steels are ferromagnetic, with the Curie temperature T_C close to the expected range of operating temperatures of a fusion power plant. The mechanical properties of steels are correlated to their magnetic properties through changes in the local microstructure, arising from irradiation and ageing. Within the miscibility gap, thermally aged Fe-Cr alloys undergo slow coherent phase separation into Cr-rich α' and Fe-rich α precipitates. This gives rise to a phenomenon known as '475°C embrittlement'[22].

In general, precipitation during isothermal ageing oc-

curs across time scales exceeding 10^4 hours[23]. Under irradiation, this is accelerated by 6 to 7 orders of magnitude due to a substantial increase in point defect concentrations, enabling faster diffusion[24]. The microstructural evolution of the precipitates have been shown to be the same during irradiation and annealing[24], except in the vicinity of point defect sinks, such as cavities and grain boundaries, which result in precipitate free zones[25,26]. For Cr concentrations below $\approx 10\%$, short range ordering of the Cr magnetic moments enforces a negative formation enthalpy[27,28]. It favours complete dissolution of Cr as there is no thermodynamic driving force to clustering and precipitation.

The kinetics of precipitate formation has been widely studied through both experimental[23,29–33] and theoretical approaches[24,33,34]. However, magnetic effects are largely omitted. This motivates a systematic investigation on model Fe-Cr alloys with different microstructures representative of irradiated steels. Such investigations may lay the foundation towards the development of non-invasive experimental methods to determine Cr precipitation through magnetic properties. Towards this aim, the first part of this paper introduces the method of spin dynamics, the Hamiltonian, the quantitative properties of interest, and the benchmarking results, comparing them with Monte Carlo Magnetic Cluster Expansion (MCE) simulations. A comprehensive investigation into the magnetic effects is then undertaken, including the change in T_C with composition and Cr clustering. The correlated behaviour of magnetic moments (or atomic spins) and its affect on the susceptibility are discussed for spherical Cr precipitates and (001) interfaces.

II. METHODOLOGY

A. Spin Dynamics

Spin Dynamics (SD) is an indispensable tool for the study of magnetic excitations. Originating from the Landau-Lifshitz and Gilbert equations[35,36], SD has vastly extended our understanding of solitons and magnons in magnetic media[15,37,38]. Recent developments consider both the direction and magnitude of an atomic spin as a three dimensional vector[39,40]. Transverse and longitudinal fluctuations are treated within a unified framework, corresponding to the localised and itinerant property of hybridised s and d electrons[41].

Spin temperature can be regulated using Langevin thermostat[39,42–44]. Considering an arbitrary spin Hamiltonian $\mathcal{H}$, the Langevin equation of motion of atomic spin $\mathbf{S}_i$ can be written as[39]:

$$\frac{d\mathbf{S}_i}{dt} = \frac{1}{\hbar}\left(\mathbf{S}_i \times \mathbf{H}_i\right) + \gamma_s \mathbf{H}_i + \boldsymbol{\xi}_i, \quad (1)$$

where the effective field $\mathbf{H}_i$ for spin i:

$$\mathbf{H}_i = -\frac{\partial \mathcal{H}}{\partial \mathbf{S}_i}. \quad (2)$$

γ_s is a damping parameter and $\boldsymbol{\xi}_i$ is δ-correlated random noise, which satisfies $\langle \boldsymbol{\xi}_i(t) \rangle = 0$ and $\langle \xi_{i\alpha}(t)\xi_{j\beta}(t') \rangle = \mu_s \delta_{ij}\delta_{\alpha\beta}\delta(t - t')$. Greek alphabet subscripts represent Cartesian coordinates. According to the fluctuation-dissipation theorem (FDT)[45,46], one can obtain a relationship between random and dissipative forces[39,47], namely $\mu_s = 2\gamma_s k_B T$. The magnetic moment is related to atomic spin by a simple expression:

$$\mathbf{M}_i = -g\mu_B \mathbf{S}_i, \quad (3)$$

where g is the electronic g-factor and μ_B is the Bohr magneton.

In this paper we use the implementation of SD within our code SPILADY[48]. The source code has been generalised to handle multiple elemental species and complex Hamiltonian forms. For all calculations, the equation of motion is integrated using the parallelised symplectic Suzuki-Trotter decomposition algorithm[40] with a time step of 1fs.

B. Magnetic cluster expansion Hamiltonian

We employ the functional form and parameters of a Heisenberg-Landau type magnetic cluster expansion (MCE) Hamiltonian, which was developed for Monte Carlo simulations[49–52] of $Fe_{1-x}Cr_x$ alloys. Terms in the MCE Hamiltonian, contributing to the effective field, can roughly be decomposed into inter-site interaction 'Heisenberg' terms $\mathcal{H}_H$ and on-site 'Landau' $\mathcal{H}_L$ terms:

$$\mathcal{H} = \mathcal{H}_H + \mathcal{H}_L, \quad (4)$$

where

$$\mathcal{H}_H = \sum_{i \neq j} \left(J_{ij}^{(0)} + J_{ij}^{(1)}(\sigma_i + \sigma_j) + J_{ij}^{(2)}\sigma_i\sigma_j \right)\mathbf{M}_i \cdot \mathbf{M}_j, \quad (5)$$

and

$$\mathcal{H}_L = \sum_i \left(A^{(0)} + A^{(1)}\sigma_i + \sum_{j \neq i} A_{ij}^{(2)}\sigma_i\sigma_j \right)\mathbf{M}_i^2$$
$$+ \sum_i \left(B^{(0)} + B^{(1)}\sigma_i + \sum_{j \neq i} B_{ij}^{(2)}\sigma_i\sigma_j \right)\mathbf{M}_i^4 \quad (6)$$

The energy of an alloy configuration depends on atomic site occupational variables σ_i and the non-collinear magnetic moments of each atom $\mathbf{M}_i$. The discrete occupational site variable σ_i takes a value of $\sigma_i = +1$ or $\sigma_i = -1$ depending on whether the ith site is occupied by an Fe or Cr atom, respectively.

The MCE Hamiltonian is explicitly dependent upon the local atomic configuration up to the 5th coordination shell, which reflects the dependency of magnetic properties on the local environment. Since the magnetic degrees of freedom are not independent of the atomic configuration, both the magnetic order and magnitudes[53] are dependent upon the atomic configuration via the quadratic

	1st	2nd	3rd	4th	5th
$J_{ij}^{\text{Fe-Fe}}$	-3.097	-2.426	0.0	0.0	0.0
$J_{ij}^{\text{Fe-Cr}}$	5.555	6.890	3.432	6.984	7.374
$J_{ij}^{\text{Cr-Cr}}$	19.881	12.380	-0.266	-2.322	0.0
X	$X^{(0)}$	$X^{(1)}$	$X_{1nn}^{(2)}$	$X_{2nn}^{(2)}$	
A	-94.513	-44.225	-4.652	4.601	
B	46.56	-18.864	0.201	-1.738	

TABLE I. Magnetic interaction parameters J_{ij}, A and B of the Magnetic Cluster Expansion Hamiltonian (Ref. 51). Environment dependence of the Hamiltonian arises from the site occupation variables σ_i, where $\sigma_{\text{Fe}} = +1$ and $\sigma_{\text{Cr}} = -1$. For example, the quadratic Landau term for Fe becomes $A(\text{Fe}) = A^{(0)} + A^{(1)} + 6A_{1nn}^{(2)} + 8A_{2nn}^{(2)} = 148.35\text{meV}$ and the exchange coupling parameter between the 1st nearest neighbour of Fe and Cr is $J_{1nn}^{\text{Fe-Cr}} = J_{1nn}^{(0)} + J_{1nn}^{(1)}(1 + (-1)) + J_{1nn}^{(2)}(1 \times (-1)) = 5.555$ meV.

and quartic Landau coefficients A_i, B_i and the Heisenberg exchange coupling parameter J_{ij}. The exchange parameters are parameterised up to the 5th nearest neighbour. The Landau type coefficients $A^{(2)}$ and $B^{(2)}$ are effected by neighbours in the 1st and 2nd coordination shells. The numerical values attributed to the parameters for the $\text{Fe}_{1-x}\text{Cr}_x$ Hamiltonian in Eq. 4 are given explicitly in Table I. Details regarding the parametrisation are given in Refs. 49 and 51.

C. Simulation Metrics

An important macroscopic order parameter is the averaged over time magnetic moment. The contribution by species $\eta = $ Fe or Cr is calculated using the magnetic moments in thermal equilibrium at a particular temperature T over the trajectory in a period of τ, assuming ergodicity:

$$\langle \mathbf{M}_\eta \rangle = \frac{1}{\tau} \int_0^\tau \left(\frac{1}{N_\eta} \sum_i^{N_\eta} \mathbf{M}_i(t) \right) dt. \quad (7)$$

The summation spans all atoms N_η of the species. The averaged system magnetic moment is the contribution from all element types. Magnetisation is the magnitude of the averaged magnetic moment i.e. $\bar{M}_\eta = |\langle \mathbf{M}_\eta \rangle|$.

The susceptibility of an observable with respect to its conjugate field can be calculated from the fluctuations of the observable within a canonical ensemble. This facilitates the calculation of the magnetic susceptibility χ through the spin dynamics calculations:

$$\chi = \mu_0 \frac{\langle \mathbf{M}^2 \rangle - \langle \mathbf{M} \rangle^2}{k_B T}, \quad (8)$$

where μ_0 is the vacuum permeability and $\mathbf{M}$ is the averaged magnetic moment within a defined volume.

One can estimate the fundamental timescales of magnetic excitations using the correlation of fluctuating magnetic moments. The correlation of a magnetic moment at site i over a time interval of τ from a starting time t can be calculated using a time-displaced spin-spin autocorrelation function.

$$c_0(\mathbf{r}, \tau) = \frac{1}{N} \sum_n^N \left\langle \mathbf{e}_i(\mathbf{r}, t + \tau) \cdot \mathbf{e}_i(\mathbf{r}, t) \right\rangle, \quad (9)$$

where $\mathbf{e}_i = \mathbf{M}_i / M_i$ is the unit vector of magnetic moment. The autocorrelation function is calculated on-the-fly[54] at thermal equilibrium and averaged using multiple statistically independent starting times.

The time-displaced correlated behaviour between the ith magnetic moment and the magnetic moments constituting its 1st coordination shell gives insights into the magnetic ordering and timescale of its decoherence:

$$c_1(\mathbf{r}, \tau) = \frac{1}{8N} \sum_n^N \left\langle \sum_{j=1}^8 \mathbf{e}_j(\mathbf{r}', t + \tau) \cdot \mathbf{e}_i(\mathbf{r}, t) \right\rangle, \quad (10)$$

where atom j is in the 1st nearest neighbour shell of atom i. At cryogenic temperatures, a FM monodomain would yield $c_1 = 1$ whereas a layered AFM domain such as in L1_0 FeNi would return $c_1 = -1$.

In the following, when we consider a spherical precipitate, we measure the averaged correlation functions of magnetic moments displaced from a chosen origin $\mathbf{r}_0$, i.e. the geometric centre of a cluster. We called $c_0(|\mathbf{r} - \mathbf{r}_0|)$ the radially resolved time-displaced spin-spin autocorrelation functions (RRACF), and $c_1(|\mathbf{r} - \mathbf{r}_0|)$ the 1st nearest neighbour radially resolved time-displaced spin-spin correlation functions (1nRRCF).

III. BENCHMARKING MCE HAMILTONIAN IMPLEMENTATION

A. Pure bcc Fe

In order to verify the correctness of the implementation of the MCE Hamiltonian in Langevin SD, we benchmarked some key results against the work of Lavrentiev *et al.*[49,55] In their work, the ensemble averages were generated by exploring phase space through Monte Carlo method. On the other hand, Langevin SD (Eq. 1) guarantees the energy distribution at equilibrium being a Gibbs distribution through the fluctuation and dissipation forces according to the FDT[39,42,45,46].

Bulk bcc Fe was modelled using a simulation cell containing 31250 atoms constructed from $25 \times 25 \times 25$ primitive unit cells. Periodic boundary conditions are enforced. The system was heated over a temperature range from 100K to 1500K in 100K intervals and reduced to 20K in the vicinity of the T_C. Statistics were gathered during a 5ps production run following a 1ps thermal equilibration period during which ensemble properties converged. Comparative results are shown in Fig. 1 giving
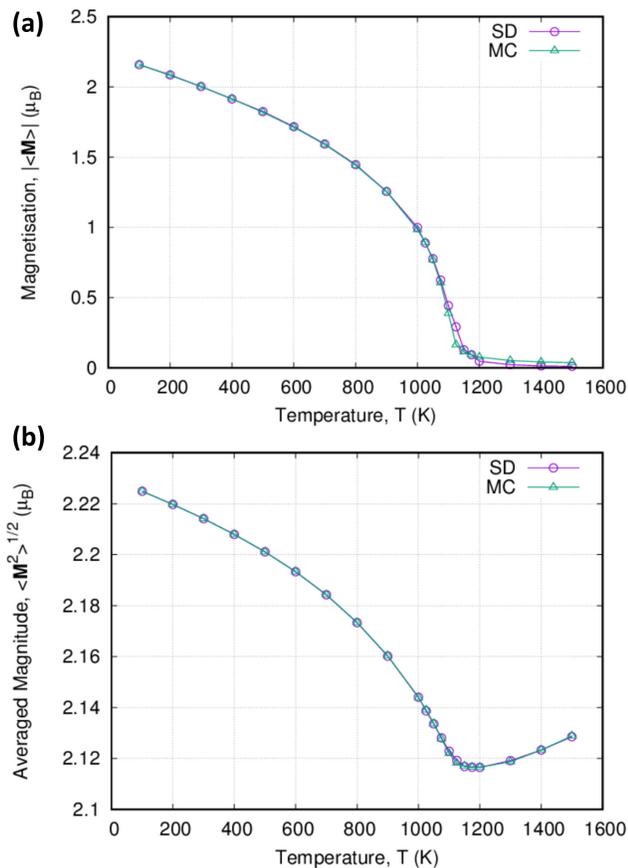
FIG. 1. Comparison between time averaged spin dynamics against Monte Carlo (MC) sampling[49], both implementing the magnetic cluster expansion (MCE) Hamiltonian (Eq. 4) for (a) the magnetic moment of pure Fe and (b) the averaged magnitude of the Fe magnetic moments against temperature. One can see excellent agreement between the two methods. A small discrepancy can be observed around the T_C. It can be accounted for by the larger system size being employed for spin dynamics simulations, which permits longer wavelength magnons. We used a box size of $25{\times}25{\times}25$ unit cells box for spin dynamics simulation, where $16{\times}16{\times}16$ unit cells box were used for MC MCE simulations.

nearly identical results for the total magnetic moment (Fig. 1(a)) and the averaged magnitude of the Fe magnetic moments (Fig. 1(b)) as a function of temperature between our calculations and Ref. 49. A slight deviation near T_C is observed, which can be accounted for by the larger system size used in this study, permitting longer wavelength magnons.

The magnetisation is maximised at low temperatures, where $\bar{M} = |\langle \mathbf{M} \rangle| = 2.16\mu_B$, at 100 K in a collinear FM state. The magnetisation decreases when temperature increases. On the approach to the T_C, the alloy becomes paramagnetic. In both methods, T_C is overvalued relatively to the experimentally observed temperature of 1045K by approximately 50K. The averaged magnitude of the magnetic moments $\langle \mathbf{M}^2 \rangle^{1/2}$ is minimum at

T_C. It is $2.117\mu_B$ at T_C, reduced from $2.23\mu_B$ at 0K. This is in good agreement with experiment[56], tight binding theory[21], MC MCE simulations[49], and previous SD simulations[39] performed using a different set of parameters.

B. Fe$_{1-x}$Cr$_x$ solid solutions

The second benchmark test is on Fe$_{1-x}$Cr$_x$ solid solutions. Simulations on iron rich solid solutions are compared to MC results[55] for $0.032 \leq x \leq 0.5$. Cr atoms are distributed randomly in Fe forming disordered solid solutions. The simulation box setup is similar to the previous pure Fe benchmark test. Samples are thermalized to 25K corresponding to Ref. 55.

The averaged system magnetic moment, and the averaged magnetic moment of the constituent Fe and Cr atoms, for different concentrations are shown in Fig. 2(a). Each data point is calculated using three different randomly generated configurations, but with the same composition. They are compared to data in Ref. 55 (connected triangles). Our SD results are in good agreement with MC simulations.

Fig. 2(b) to (e) show snapshots of different magnetic configurations at $T = 100$ K. Pure bcc Fe is in FM state. The axis of precession of magnetic moments aligns collinearly. In the dilute Cr limit with $x = 0.1$, the magnetic moments of Cr in bcc Fe matrix are anti-parallel to Fe magnetic moments. This corroborates with density functional theory calculations[27]. Such ordering is due to the strongest magnetic exchange between Cr and Fe in the MCE Hamiltonian[51], where $J_{1nn}^{\text{Fe-Cr}} = 19.881\text{meV}$ in comparison to $J_{1nn}^{\text{Fe-Fe}} = -3.097\text{meV}$ and $J_{1nn}^{\text{Cr-Cr}} = 5.555\text{meV}$.

Pure bcc Cr modeled by the MCE Hamiltonian adopts an AFM configuration. Although Cr is known to form an incommensurate SDW[10], AFM state has an energy indistinguishable from SDW within the error of DFT calculations[57]. Therefore, AFM state is presumed to be a reasonable reference state of bcc Cr for the current study. Our SD simulations identify a Néel temperature of Cr at 350K, which is in agreement with the MC MCE simulations[50].

Considerable evidence for non-collinear magnetic configurations in Fe$_{1-x}$Cr$_x$ alloys has been presented in recent years, even at low temperatures[53]. As a simple demonstration, Fig. 2(e) shows a snapshot of magnetic moments in a disordered solid solution of Fe-25 at.%Cr at $T = 25$K. It shows substantial non-collinearity arising to minimise the magnetic frustrations from small Cr clusters in the Fe matrix. Non-collinearity was also observed across Fe-Cr interfaces using the MCE Hamiltonian in Ref. 53. We will discuss this further in Sec. IV E.

We note that the absolute direction of magnetic moments is immaterial. Only the relative directions are important. This is because the Hamiltonian (Eq. 4) depends only on the scalar product between spin orien-
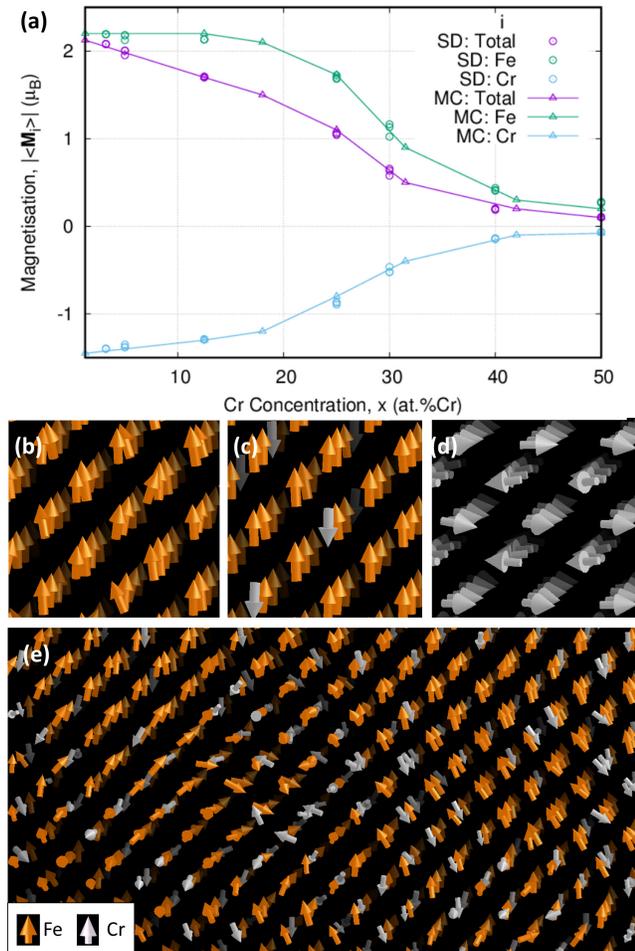
FIG. 2. Magnetic properties of $Fe_{1-x}Cr_x$ alloys simulated using spin dynamics. (a) The average magnetisation of Fe, of Cr and of the whole system of disordered $Fe_{1-x}Cr_x$ solid solutions at $T = 25K$. For each composition, three randomly generated configurations are modelled using SD (circles) and compared with Ref. 55 (connected triangles). (b) to (e) Snapshots of magnetic moments in systems with different Cr concentrations (b) Pure Fe at 100 K, in a ferromagnetic state. (c) $Fe_{0.9}Cr_{0.1}$ at 100 K. Cr moments are anti-parallel to Fe moments in the dilute limit. (d) Pure Cr at 100 K, with moments ordered antiferromagnetically. (e) $Fe_{0.75}Cr_{0.25}$ at 25 K. Higher Cr concentrations leads to frustration and complex non-collinear arrangement of magnetic moments.

tations and does not include magnetic anisotropies. The energy is invariant in spin-space to the simultaneous rotation of all moments about an arbitrary axis. The two benchmarking tests show excellent agreement between the MC and SD simulation using the same MCE Hamiltonian. In the following sections, we apply Langevin SD to study the magnetic properties of Fe-Cr alloys with different microstructures.

IV. RESULTS AND DISCUSSION

A. Disordered Solid Solutions

We start our investigation with disordered solid solutions of $Fe_{1-x}Cr_x$ with $0 \leq x \leq 0.25$. We study the effect of varying Cr composition on the T_C through the magnetic susceptibility. SD calculations were performed using a cubic simulation cell with periodic boundary conditions containing 31250 atoms.

Collinear ordering of magnetic moments along [001] was chosen for the initial configuration, allowing us to define the magnetisation axis parallel to the z direction. Statistics were collected over a 5ps production run following a 1ps thermal equilibration period. Each configuration was generated by random substitution of Cr atoms into the bcc Fe matrix to satisfy the concentration requirements. As we are using a large simulation cell for the solid solution calculations, we assume sufficient statistical sampling of local structure. To check this assumption, for x=15 and 25 at.%, we simulated three random configurations and found comparable results for each case.

The magnetisation of the disordered solid solutions are shown in Fig. 3(a) over a temperature range of 100K $\leq T \leq 1500K$. At low temperatures, the magnetisation decreases as the Cr concentration increases. The magnetisation profiles are similar to pure Fe as the temperature is raised. The magnetisation is found to remain finite for $x=$ 5 and 9 at.% at a temperature higher than the T_C of pure Fe.

We determine the T_C through the turning point in the bulk susceptibility ($\partial_T^2 \chi = 0$) as shown in Fig. 3(b). The T_C is plotted against the Cr concentration in Fig. 3(c). It is compared against experimental data and MC calculations using the MCE Hamiltonian[12]. In MC simulation, they determine the T_C through observation of peak in the specific heat instead. Excellent agreement is found between our SD calculations and the MC results. Both of them show the same trend with experiment.

The T_C increases for small Cr concentrations until 5 at.%Cr. Further increases in the Cr concentration decreases the T_C. This is in agreement with experimental observations that T_C is maximised for a Cr concentration of around 6 at. %[12,58].

We note the consolute temperature is approximately 900K. Therefore, disordered solid solutions are appropriate stable configurations near the T_C for aged Fe-Cr steels across the full compositional range. The increase in the T_C has been previously determined to be caused by the strengthening of the Fe FM ordering due to the AFM coupling from lone Cr nearest-neighbours[12,27,51].

B. Fe-Cr Alloys with idealised Cr Precipitates

Irradiation alters the microstructure of steels. Different microstructures may affect the magnetic properties,
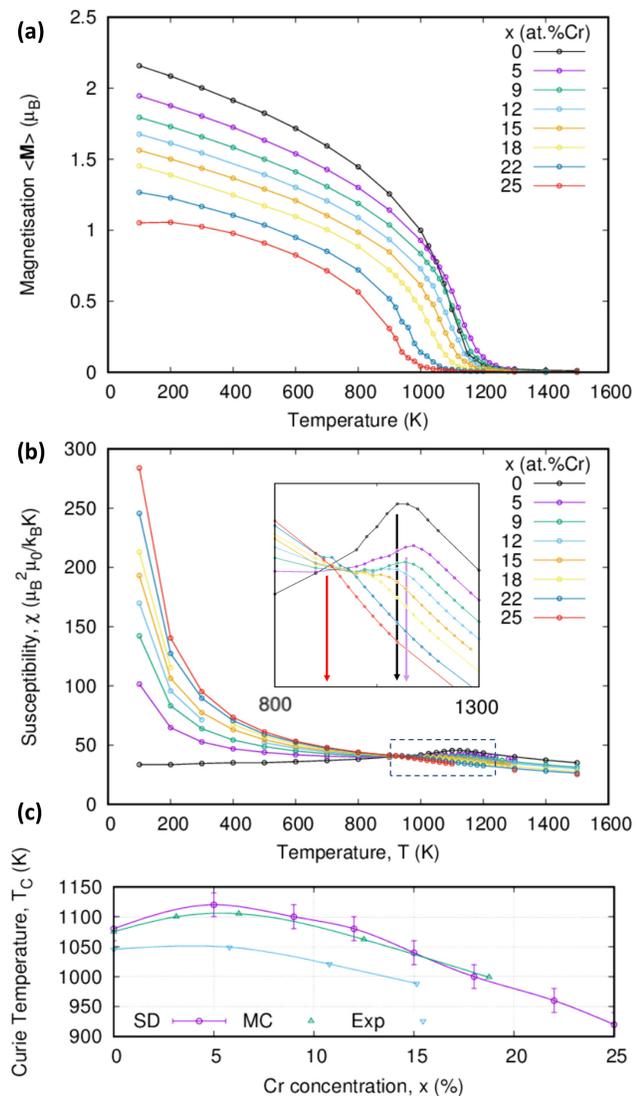
FIG. 3. Magnetic properties of disordered $Fe_{1-x}Cr_x$ solid solutions with different Cr concentrations. (a) Magnetisation with temperature. (b) Magnetic susceptibility (Eq. 8). Inset: Susceptibility around the Curie temperature T_C. The points of inflection for $x = 0$, 5 and 25 at.%Cr are indicated by arrows . (c) Curie temperature T_C variation with Cr concentration as determined from the susceptibility. Data from Monte Carlo calculations and experiment[12] are given for comparison. The determination of T_C presented in Ref. 12 is via observation of peak in the specific heat. Error bars are set as the temperature interval in sampling, which is 20K.

and vice versa, even when the nominal chemical composition is the same. In this section, we investigate how the formation of idealised α' precipitates might change the magnetic properties with respect to the disordered solid solutions investigated in Sec. IV A.

Atom probe experiments have identified that precipitates formed during ageing and irradiation start as elongated coagulated clusters and become roughly spherical over time[23]. To model this topology, simulation cells are constructed to contain 31250 atoms on ideal bcc Fe lattice sites. Atoms within a selected radius $r_c = |\mathbf{r} - \mathbf{r}_0|$ are substituted with Cr to form an α' spherical cluster. The remaining Cr substitutions necessary to form a nominal composition of x at.% are distributed randomly throughout the remaining Fe matrix. Our default system size corresponds to an α' number density of 2.7×10^{23} m^{-3} which is comparable to the lower limits observed experimentally in neutron irradiated Fe-Cr steels[59]. Clusters are generated with radii from 6 to 26Å for nominal concentrations of 9, 12, 15, 18, 22 and 25 at.%. The cluster sizes are chosen to be comparable to precipitates aged from 10 to 10000 hours[23,59].

The averaged magnetisation for selected concentrations with increasing precipitate sizes are shown in Fig. 4. For each concentration, the averaged magnetisation is shown against the magnetisation of bulk Fe ($|\langle \mathbf{M}_{Fe} \rangle|$), the bulk curve scaled proportional to the nominal concentration ($(1-x)|\langle \mathbf{M}_{Fe} \rangle|$) and the magnetisation of the disordered solid solution ($r_c = 0$). At low temperatures, the configuration in which the magnetisation is smallest is the disordered solid solution. Cr atoms attempt to magnetically order antiparallel to neighbouring Fe atoms which acts to reduce the total moment. The averaged magnetisation increases with larger cluster sizes. The scaled Fe curve gives an approximate limit obtained upon complete phase segregation as would be expected within the spinodal decomposition.

Within the α' clusters, the Cr magnetic moments order antiferromagnetically and perpendicular to the alignment of the Fe moments in the α phase. This is shown in Fig. 5(a)-(c) for the 9 at.% simulation containing a precipitate of radius 18Å. The Figures were produced using V_Sim. Cr situated directly on the cluster interface have their moments aligned antiparallel to Fe. The Cr atomic magnetic moments gradually rotate to be perpendicular to the Fe moments towards the centre of the cluster. The Cr attempts to maintain almost antiparallel ordering to their Cr nearest neighbours whilst tiling from the Fe. This is visualised in the magnetic moment space (Fig. 5(d)-(e)) where the tip of the vector of each magnetic moment centred on the origin is plotted as a dot. The bulge at the base reveals the magnetic moments of Cr are strengthened when surrounded by Fe.

Non-collinear arrangements similar to those in the cluster have previously been observed across (001) and (011) Fe-Cr interfaces[12,60]. Our simulations on clusters show that these magnetic configurations are quite general and exist even for high index interfaces and at elevated temperatures as a method to minimise frustration and satisfy local magnetic order. This highlights the need for consideration of non-collinear magnetism in future studies.

At high temperatures the difference in magnetisation between alloys of the same nominal concentration remains significant. To emphasise this, in Fig. 6, we plot the magnetisation for different concentrations at 600K and 800K. The lower limit is taken as the magnetisation of the disordered solid solution configuration. The upper
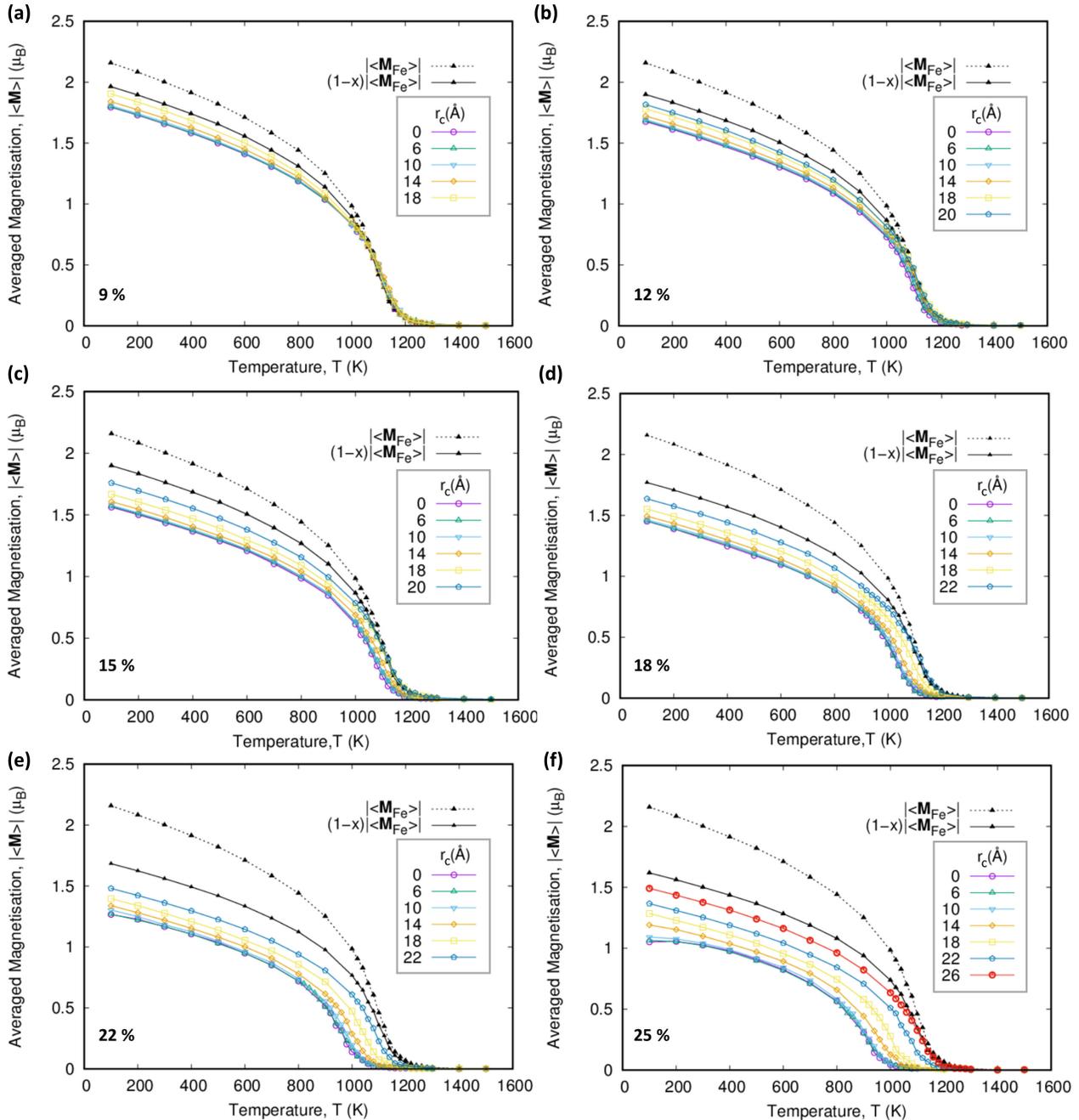
FIG. 4. Averaged magnetisation of Fe-Cr alloys as a function of temperature, concentration and cluster size. All precipitates are spherical clusters in bcc α' phase with a local concentration of 100% Cr. Remaining Cr required to construct supercells with overall concentration x are dispersed randomly in the Fe-matrix. System Cr concentrations x of (a) 9% (b) 12% (c) 15% (d) 18% (e) 22% (f) 25% for radii of 6 to 26Å. A radius of 0Å corresponds to a disordered solid solution.

limit occurs with complete phase segregation, which has the same magnetisation as the bulk Fe case scaled according to the Cr concentration. Current fusion reactor designs expect the first wall to operate within the temperature range between 350°C and 550°C[4] (620-820K) and be constructed from steels with 9 at.%Cr such as EUROFER-97. For this concentration, our SD simulations show the magnetisation can change up to 10.4% at

600K and 10.3% at 800K, from changes in non-defective microstructure alone.

A general trend observed is that T_C is comparatively higher for systems with larger precipitates. Simulations where large clusters remain ferromagnetic at temperatures higher than bulk Fe are particularly apparent in cases with dilute concentrations. In Fig. 7, T_C as a function of nominal composition and cluster size is pre-
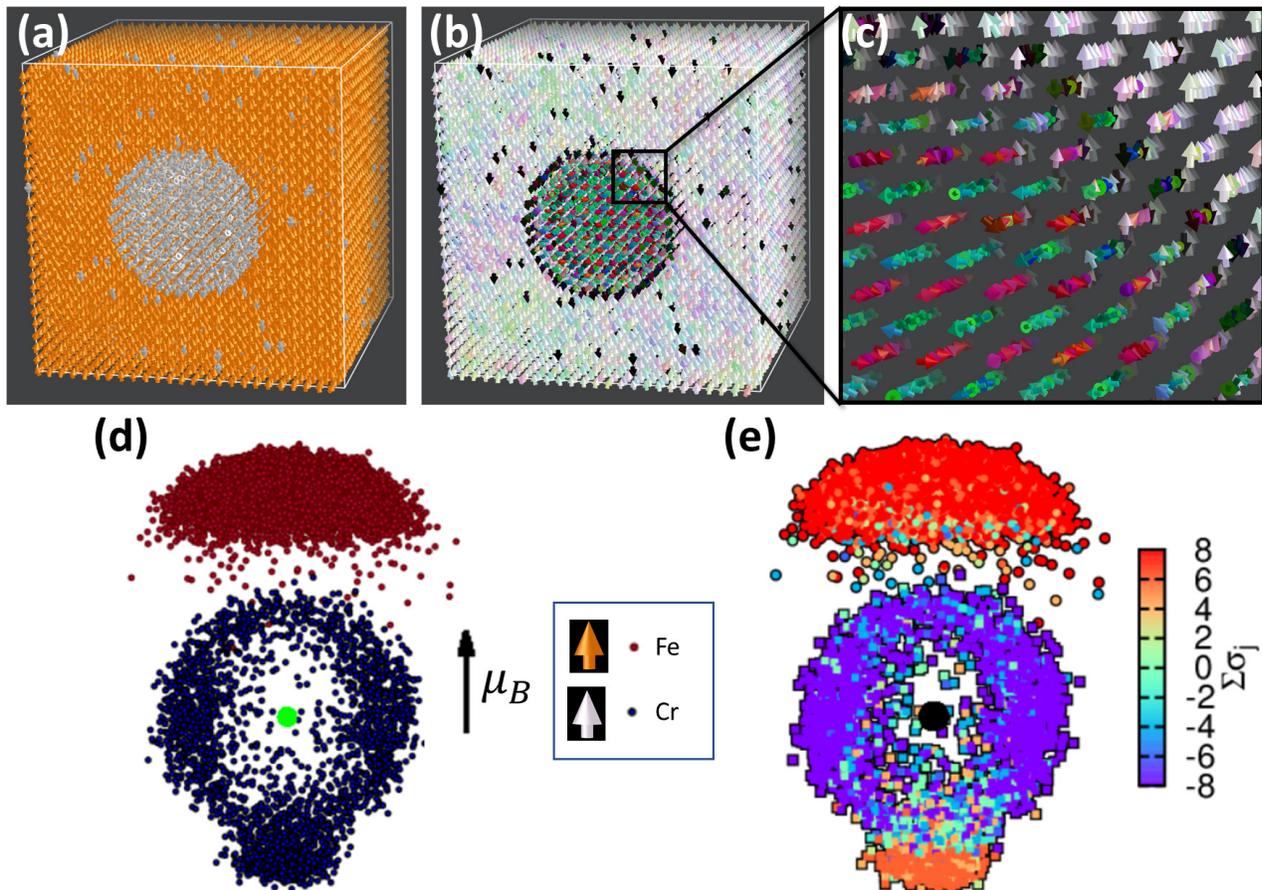
FIG. 5. Magnetic moments of a spherical α' precipitate with radius = 18Å at $T = 100$K. The overall chemical composition contains 9 at.% Cr. An instantaneous snapshot is taken at the final time step of the production run. (a) Magnetic moments of Fe (orange) and Cr (white). (b) Magnetic moments colourised using double conical space. (c) Focused view near the interface. (d) Magnetic moment-space representation of all moments in the system at the final timestep. (e) Magnetic moment space map colourised according to the sum of the occupational site variables of the nearest neighbours (8=all Fe, 0=50%Fe-50%Cr, -8=all Cr).

sented. Again, T_C is determined as the turning point in the magnetic susceptibility. Quantitatively the resolution of this approach is limited by the temperature steps taken ($\Delta T = 20$K) and the smoothness of the calculated curve. Nonetheless, it shows the same qualitative behaviour observed in the magnetisation.

The increase of T_C can be understood to occur due to the same physical origin, which gives a maximum T_C at 6 at.% in the solid solution. As Cr atoms coalesce into clusters, the relative concentration of Cr within the α phase decreases. This increases the average number of Fe nearest neighbours and decreases the number of nearest and next-nearest neighbouring Cr atoms. As an explicit example, for 12 at.%Cr the 18Å cluster is observed to have a higher T_C than pure Fe. In total, there are 3760 Cr atoms in the simulation cell. The 18Å cluster is comprised of 2085 Cr atoms leaving 1675 dispersed in the bulk. This corresponds to an effective concentration (x') of 5.36% in the α phase which matches the solid

solution concentration in which the T_C is maximised.

C. Spatial and time resolved magnetic properties of α' precipitates

For larger cluster sizes, we can study the magnetic properties with spatial resolution. We demonstrate this by examining a spherical α' cluster in pure Fe with a radius equal to 4nm. The simulation cell contains 250,000 atoms ($50 \times 50 \times 50$ unit cells). This cell corresponds to a number density of 3.2×10^{23} m^{-3} which can be observed experimentally, such as experiments on neutron irradiated Fe-12Cr at 320°C by Reese et al.[59].

In Fig. 8 (a) the magnetic moment and (b) susceptibility for temperatures from 100K to 1500K are plotted as a function of the distance from the centre of the ideal spherical α' cluster $|\mathbf{r}-\mathbf{r}_0|$. The magnetic moments in the pure Fe surrounding a Cr cluster are found to have bulk
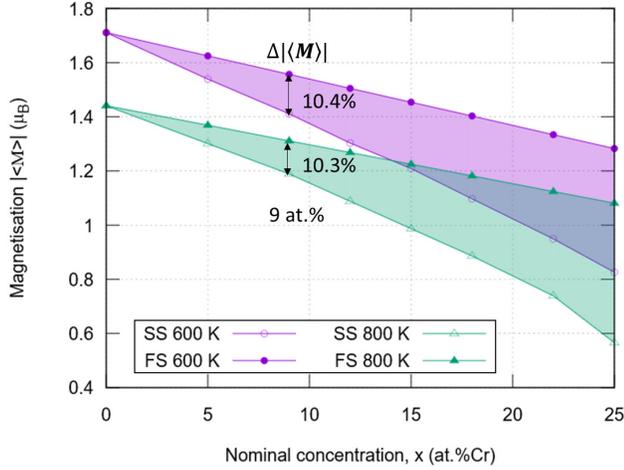
FIG. 6. Plot illustrating the effect of microstructure on the magnetisation for Fe 9 at.%Cr alloys at 600K and 800K. The lower limits correspond to the disordered solid solution (SS). The upper limits corresponds to complete phase separation (FS).
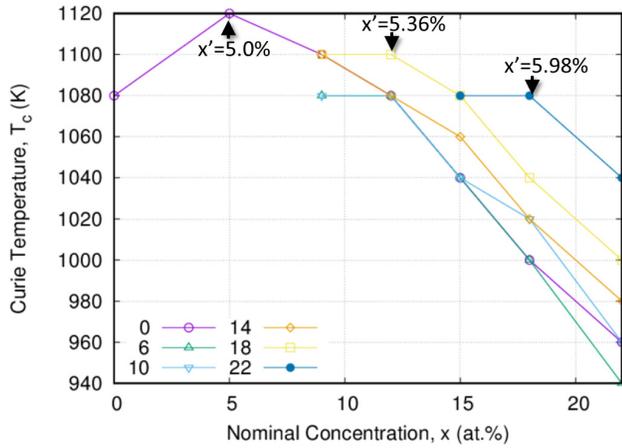
FIG. 7. Variation of the Curie temperature with respect to α' cluster size for different nominal Cr concentrations. The Curie temperature is maximised for any nominal concentration x when the effective concentration of the α is $x' \approx 5 - 6$ at.%.

FIG. 8. Magnetic properties of spherical Cr clusters of radius $r_c = 4$ nm in Fe. (a) Averaged magnetisation and (b) susceptibility. Evaluated as a function of distance $|\mathbf{r} - \mathbf{r_0}|$ from the centre of the precipitate (inset).

in the bulk of the α Fe. The disorderliness at the Fe-Cr interface leads to a reduction of T_C locally.

An advantage of SD compared to MC is its capability of simulating the dynamic time resolved magnetic properties. In Fig. 9, we plot the radially resolved autocorrelation function (RRACF, Eq. 9) and the first nearest neighbour radially resolved correlation function (1nRRCF, Eq. 10) of magnetic moments at temperatures of 100K, 500K, 800K and 1200K. They are measured at different distances from the centre of the ideal spherical α' cluster. We selected six radii to compare. Three of them are within the precipitate, 13.1Å, 35.1Å and 37.0Å. The next is at 40.1Å, which is at the first Fe layer surrounding the Cr cluster. The remaining two are at 45.0Å and 70.0Å, which are in the α phase. The profile of the correlation functions c_0 and c_1 consist of a decaying envelope function indicative of the characteristic dephasing (relaxation) time and an oscillatory component related to the correlation time. The oscillations in the RRACF are due to the precession of magnetic moments[61]. Fe moments precess at a higher frequency than the Cr moments. If the rotational frequency $\omega_i = -|\mathbf{H}_i|/\hbar$ is considered, we immediately realise the effective field is greatest on the Fe moments. Correspondingly the effective field is weak

values. When approaching the Cr-Fe interface from the α phase, the magnetisation drops when the 5th nearest neighbour coordination shells become populated by Cr atoms. The magnetic moment drops sharply within the α'. The susceptibility within the α' is observed to oscillate to a penetration depth of 1-2nm. This is due to the long range nature of the exchange coupling parameters (see Table I).

The susceptibility within the cluster is particularly high below the Néel temperature (≈ 350K) relative to the bulk Fe due to the magnetic frustration of the Cr moments. A spike in susceptibility is observed within the Fe matrix even at low temperatures. This shows that the Fe moments near the interface fluctuate more readily than

FIG. 9. Radially resolved autocorrelation and first nearest neighbour correlation functions at T =100K, 500K, 800K and 1200K. They are taken as averaged values for magnetic moments located at 13.1, 35.1, 37.0, 40.1, 45.0 and 70.0Å away from the centre of a Cr cluster in Fe with radius equals to 40Å.

where there is reduced correlation such as at 35.1Å. A correlation time of 10-20 ps is generally observed.

At T =100K the RRACF is positive for all radii. In the α phase away from the cluster, the RRACF remains close to unity indicating the magnetic moments are strongly correlated over time. The Fe moments on the interface (40.1Å) have a lower RRACF due to the magnetic frustration reducing the correlation. This coincides with the sharp increase in magnetic susceptibility along the interfacial Fe layers. Near the centre of the precipitate (13.1 Å), the Cr magnetic moments have bulk-like ordering and are strongly correlated.

Near the interface the magnetisation within the cluster fluctuates. As one can see in Fig. 8(a), the average moment peaks at 37.0Å and troughs at 35.1Å. The RRACF shows that at 100K, the moments are more correlated at 37Å where a peak is observed in the magnetic

moment (see Fig. 8a) in comparison with 35.1 Å which corresponds to a radius of reduced magnetisation. At 35.1 Å, the RRACF is weakest indicating localised frustration.

The 1nRRCF provides a measure of correlation between a magnetic moment at $|\mathbf{r} - \mathbf{r}_0|$ with its nearest neighbours. At 100K, it shows that the Fe moments in the α phase remain extremely collinear with their neighbours since $c_1 \approx 1$. Collinearity is decreased slightly for the Fe magnetic moments near the Cr cluster (40.1Å). Cr magnetic order is bulk-like near the centre of the precipitate at 13.1Å where $c_1 \approx -1$. Towards the Fe interface the Cr moments become less correlated with their nearest neighbours over time as indicated by the increased value of the 1nRRCF. This indicates the Cr moments are deviating from AFM ordering.

At 500K, Cr moments in the centre of the precipitate
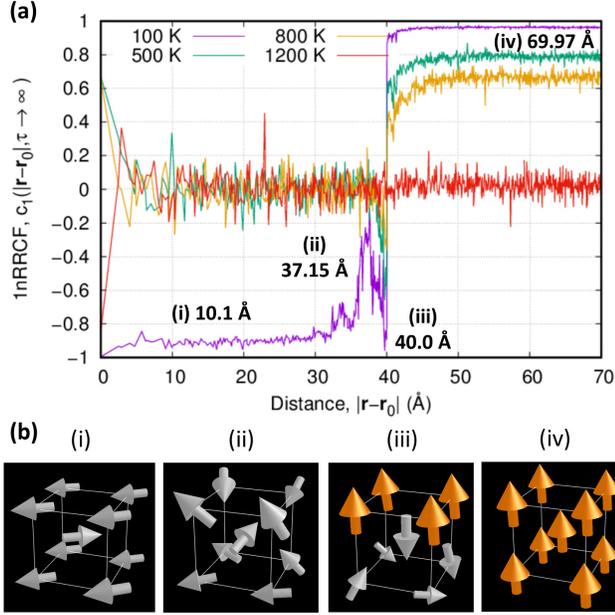
FIG. 10. (a) 1st nearest neighbour radially resolved correlation function (1nRRCF) in the long time limit as a function of radius $|\mathbf{r} - \mathbf{r}_0|$ from the centre of the Cr precipitate. The 1nRRCF is converged and plotted for time t=200ps at 100K, 500K, 800K and 1200K. (b) Averaged magnetic configurations of representative unit cells for $|\mathbf{r}-\mathbf{r}_0| =$ (i) 10.1Å, (ii) 37.15Å, (iii) 40.0Å and (iv) 69.97Å at $T = $100K.

(13.1Å & 35.1Å) have become uncorrelated, which is consistent with $T_N \approx 350$K. These moments dephase within 20-30ps. Moments at 37.0 Å from the precipitate centre are still determined to be weakly correlated with their neighbouring atoms and the 1nRRCF is found to become positive.

At 800K, the Fe magnetic moments remain strongly correlated for both RRACF and 1nRRCF measures albeit collinearity has decreased due to thermal fluctuations. Fe magnetic moments near the α' interface at 40.1Å remain less correlated than those in the Fe matrix and take longer time to dephase. These interfacial Fe moments have higher frequency oscillations identifying the effective field is stronger due to the strong J_{1nn}^{Fe-Cr} interaction. The faster fluctuations give rise to the enhanced susceptibility (eqn. 8). This provides further evidence that the effective T_C is reduced around the cluster which acts as a nucleation site for the ferromagnetic to paramagnetic phase transition.

At 1200K, all magnetic moments become incoherent, as shown by both the RRACF and the 1nRRCF tending to zero (Figure 9c). This is consistent with the loss of the net magnetisation (Fig. 8a). The dephasing time of the bulk-like Fe moments with their neighbours is approximately ten-fold greater than the Cr moments within the α' cluster.

We may have further analysis on the dynamic proper-

ties from the long-time limit of the 1nRRCF:

$$c_1(r, \infty) \to \langle \hat{\mathbf{M}}^{1nn} \rangle \cdot \langle \hat{\mathbf{M}} \rangle \qquad (11)$$

In Fig. 10(a), the 1nRRCF limit is plotted as a function of radius for 100K, 500K, 800K and 1200K. At 100K, the reduction in Cr correlation is again observed towards the interface with the sharp increase directly at the interfacial layers. Four radii of interest are selected (i) 10.1 Å (ii) 37.15 Å (iii) 40.0 Å and (iv) 69.97 Å. The time averaged magnetic moments within a representative conventional unit cell centred at each radius is shown in Figure 10(b). The distributions are in agreement to those previously inferred from the RRACF and the 1nRRCF. That is, Cr moments deep within the cluster are arranged antiferromagnetically (i) and perpendicular to the FM ordered Fe moments (iv). The magnitude of Cr moments on the interface are increased and locked antiparallel to the interfacial Fe moments with next Cr moments starting to rotate in plane (iii). A region of frustration exists within a penetration depth of 10 Å from the interface were the Cr moments are less correlated (ii).

D. Impure Cr Precipitates

In previous sections, we considered idealised spherical α' clusters. In reality, a Cr cluster is rich in Cr but impure[59]. Recent studies show the formation of Cr clusters in neutron-, ion- and electron irradiated alloys, as well as clusters in thermally aged materials, sized between 10 and 40 Å and having local Cr concentrations between 50 and 95%[59,62–64]. We investigate whether the same phenomena exhibited by pure Cr clusters are observed with impure clusters as the α' phase is diluted by Fe substitutions.

A spherical α' precipitate of concentration x_c and radius 40Å is created in a pure Fe matrix. Three samples are generated for each concentration $x_c = 0.8, 0.6, 0.4, 0.2$ in a supercell with 250,000 atoms. In Fig. 11(i), the radially averaged magnetisation and (ii) the magnetic susceptibility are plotted as a function of distance from the centre of the cluster. The region between the smallest and largest values measured for each simulation is shaded and the average of the three runs is plotted as a solid line.

At low temperatures ($T < T_C$), the magnetisation in the Fe matrix recovers the bulk values typically within 10 Å from the α' interface. When the temperature increases, the recovery length increases for all x_c. At 1100K, the recovery length is 20-30Å for all x_c, even where there is no Cr in the Fe matrix. This indicates the interactions and associated reduced ferromagnetic ordering proximate to the interface have long range effects, which reduces their correlated reinforcement.

For higher concentrations of Fe within the α', the total magnetisation within the cluster steadily increases. A discontinuous change in the radially averaged magnetisation is observed across the interface. The total magneti-
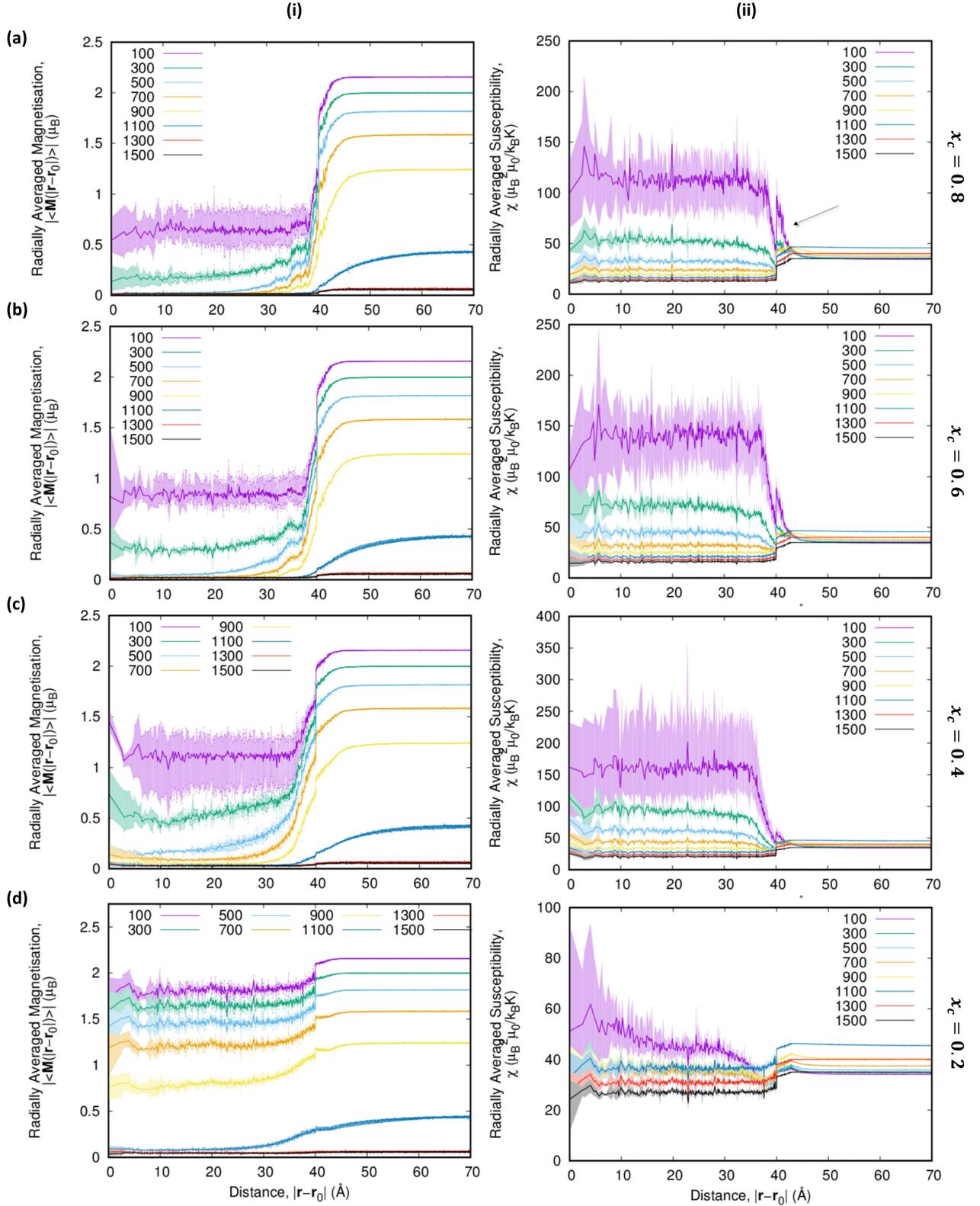
FIG. 11. (i) Radially averaged magnetisation and (ii) magnetic susceptibility as a function of radius from the centre of a spherical α' cluster with radius of 40Å. The Cr precipitate has a concentration of (a) 80 at.%Cr, (b) 60 at.%Cr, (c) 40 at.%Cr and (d) 20 at.%Cr. Three samples are simulated for each case. The averaged value is shown as the solid line. The region between the smallest and largest values measured for each simulation is shaded.
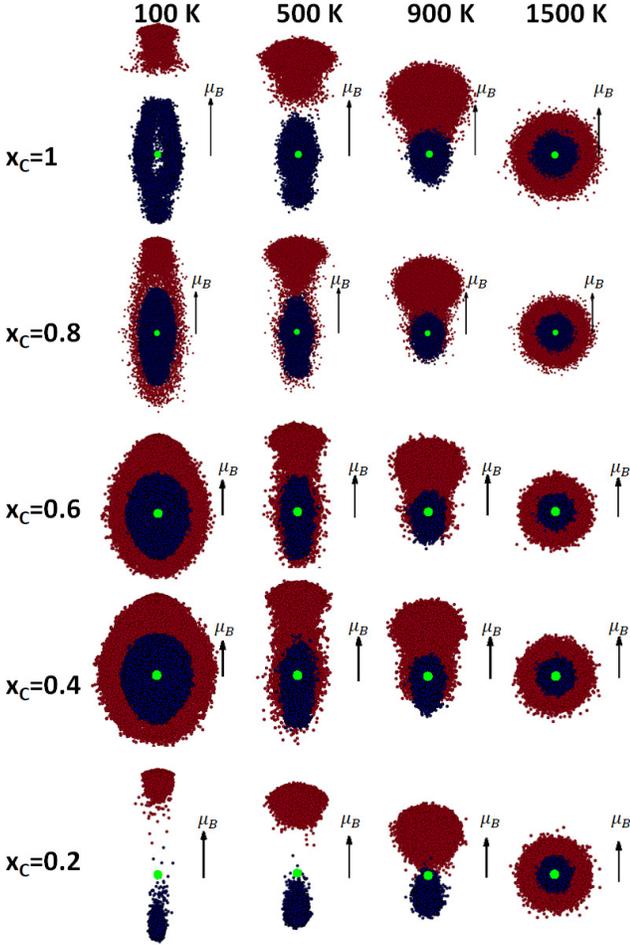
FIG. 12. Time averaged magnetic moment space diagrams for the Cr clusters of different local concentrations considered in Fig. 11 at 100K, 500K, 900K and 1500K. Dots correspond to origin centred Fe moments and blue for Cr. Each map is shown with respect to a scale of $1\mu_B$. Magnetic moments were averaged over every time step during the 5ps production run.

sation is enhanced within 10Å of the precipitate interface.

The enhanced magnetic susceptibility of the Fe atoms near the interface discussed in the previous section is also observed for the non-ideal clusters (see arrow in (iia)). When the local Cr concentration decreases, the enhancement decreases. Nonetheless, for the $x_c = 0.2$ case the susceptibility of Fe on the interface is still increased relative to the rest of the α phase. This indicates that α' acts as a nucleation site for the phase transitions even for dilutely concentrated Cr clusters.

Within the cluster, the susceptibility is reduced near the interface. This corresponds to an increased effective T_N originating from the interfacial Cr coupling to Fe moments.

To visualise the magnetic ordering in the system and its changes with temperature, the magnetic moment space for each precipitate concentration is shown in Fig.

12. The moments are averaged over every timestep during the SD simulations. For $x_c = 1$ the Cr magnetic moments in the centre of the cluster arrange with antiferromagnetic ordering perpendicular to the magnetisation axis of the Fe as was shown in Fig. 5. As the temperature increases, the moments become more disordered. Nonetheless, at 500K, which is above T_N, Cr moments retain some ordering parallel to the Fe magnetisation axis indicated by the prolated distribution. At 1500K, when temperature is well above T_N and T_C, the moments of Fe and Cr are spherically distributed indicating a paramagnetic state.

For mid to low concentrations of Fe dispersed within the α' precipitate, the moment space experiences significant frustration generating an egg-shaped/ovoid distribution. The Fe moments maintain weak ordering with a net magnetisation and with maxima along the major axis of the ovoid. The Cr moment distribution is orientated opposite to that of Fe. At 500K, the thermal agitation enables the unfavourable components of the Fe moments perpendicular to the magnetisation axis to uncouple and reorientate to be parallel. When $x_c = 0.2$, AFM ordering between the Cr and Fe becomes prominent minimising the transverse components of the magnetic moments at all temperatures.

In summary, the idealised pure Cr precipitates have an ordered non-collinear AFM structure which becomes more disordered with Fe substitutions. Despite the loss of magnetic ordering, the overall properties remain similar. The effective T_C of Fe surrounding the precipitate is reduced whereas T_N of interfacial Cr atoms is increased. This results in a spatial dependence of time-resolved properties such as the susceptibility which finds the interfacial Fe to be more susceptible than Fe in the α phase.

E. Ideal (001) Interface of Fe-Cr Superlattices

For large clusters, we may approximate the interface by ideal flat interfaces with different orientations. In this section, we study the magnetic structure of a (001) Fe/Cr interface. Spin dynamics calculations were performed on a cell containing 32000 atoms, where $20 \times 20 \times 20$ Cr unit cells stacked upon $20 \times 20 \times 20$ Fe unit cells. Periodic boundary conditions are enforced. Essentially, we created an Fe/Cr superlattice with two interfaces in the principle cell. Certain magnetic properties of such an ensemble has been studied using MC MCE simulations in Ref. 53. Using SD, we can study the continuous evolution of magnetic moments as a function of time. We investigate the time correlation across the interfaces and compare it with the more complex configurations investigated for the clusters.

In Fig. 13(a), the averaged magnetisation of the system as a function of temperature is shown. The magnetisation almost equals to the scaled value for bulk Fe implying the Fe magnetic moments in the Fe layers re-
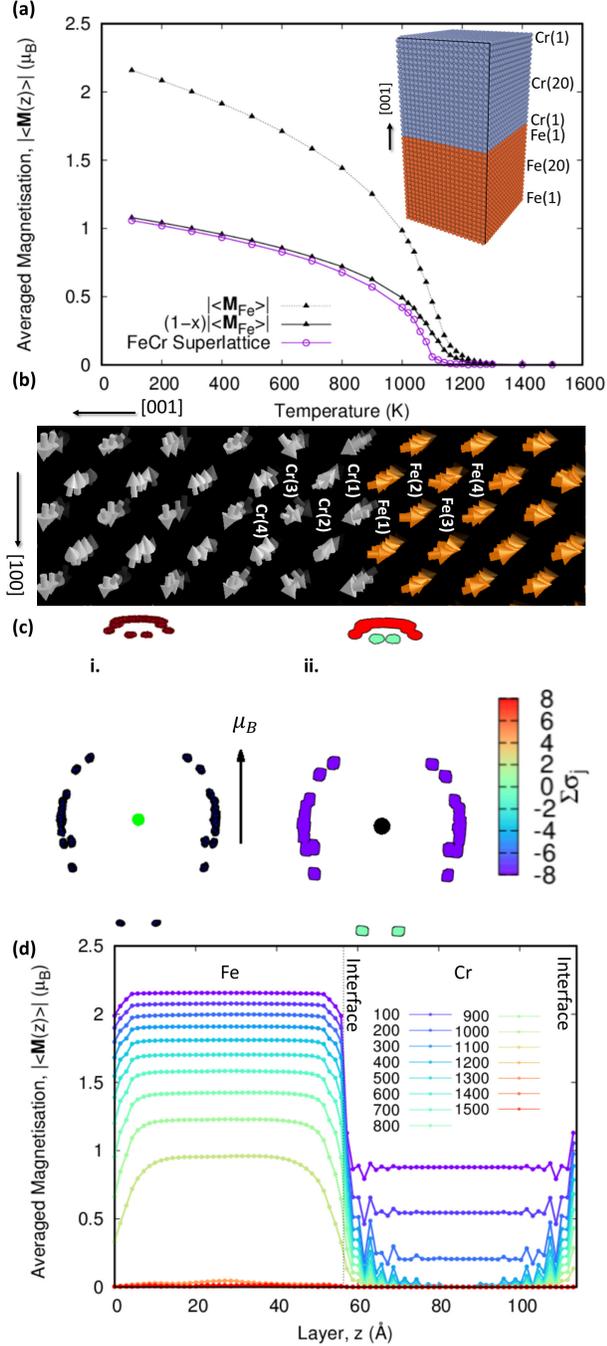
FIG. 13. Magnetic properties across a (001) Fe-Cr interface. (a) Magnetisation with respect to bulk Fe and with bulk Fe scaled proportional to the nominal concentration (50 at.%Cr). (b) Snap-shot of the magnetic moments at the interface at 100K. Fe magnetic moments are in orange. Cr are in grey. (c) Magnetic moment space diagram for the interface system at 100K (i) Coloured with respect to atom type. Blue corresponds to Cr moments. Red corresponds to Fe, and (ii) the sum of the nearest neighbours occupational site variables. (d) Layer averaged magnetisation for each (001) layer as a function of temperature.

main bulk like at low and intermediate temperatures. It is similar to case of large clusters with high concentration of Cr.

In Fig. 13(b), a snapshot at the final time step of the magnetic moments is plotted for a subset of atoms near the interface at 100K. We may compare it with previous MC MCE simulations[53]. Excellent agreement is found between our simulations and those given in Fig. 6 of Ref.53 at 1K. The Fe moments remain collinear whereas the orientation of the Cr moments are strongly dependent upon their proximity to the interface where they have a larger proportion of Fe in their first 5 coordinate shells. The first interfacial Cr layer is orientated antiparallel to the Fe moment alignment. Deeper into the α' the Cr magnetic moments reorientate until perpendicular to the Fe. Each Cr sublayer is approximately antiparallel to one another.

In Fig. 13(c)i, the magnetic moment space is plotted for all atoms in the simulation cell. A point is plotted at the tip of the magnetic moment vector centred on the origin finding quantitative agreement with those in Fig. 7 of Ref. 53. We note only contributions from one of the two interfaces were plotted by Lavrentiev et al.[53]. In Fig. (c)ii, each point is plotted with a colour relative to the sum of the occupational site variables σ of the atoms in the first coordination. This identifies the Fe moments near the interface are slightly tilted from collinearity. Further, the Fe moments on the interfacial layer have suppressed magnitudes.

At higher temperatures, the magnetisation of the interfacial system is observed to reduce faster than the bulk Fe. We can infer the T_C is reduced by approximately 100K (Fig. 13(a)). The layer averaged magnetisations are shown in Fig. 13(d) as a function of temperature. In the middle Cr layers, the averaged magnetisation vanishes between 300 and 400K corresponding to the Néel temperature ($T_N \approx 350$ K). A finite averaged moment in Cr is observed within a penetration depth of up to 20Å for all temperatures $< T_C$. The middle layers of the Fe recover bulk magnetisation values at low temperatures. For Fe in layers close to the interface, the magnetisation is suppressed. It is in agreement with Fig. 13(c)ii and Fig. 11 of Ref. 53. The bulk magnetisation recovery length from the interface increases with temperature.

In Fig. 14, the susceptibility resolved for each (001) layer in the simulation cell is shown between 100 and 1500K with 100K increments. Remarkable similarity is observed with respect to the ideal α' cluster (Fig. 8(b)). Again enhanced susceptibility is identified for the Fe moments near the Fe/Cr interface. It becomes clear that Cr destabilises the Fe ordering near an interface whether of low or high index.

Supporting evidence can be drawn from the time correlation functions (Eq. 9 and 10) which are now defined to be resolved per (001) layer in Figure 15. Each layer is labelled by the elemental type occupying the layer (either Fe or Cr) and a number indexing the layers proximity to the interface, such as Fe(1) or Cr(4). Index 1 represents
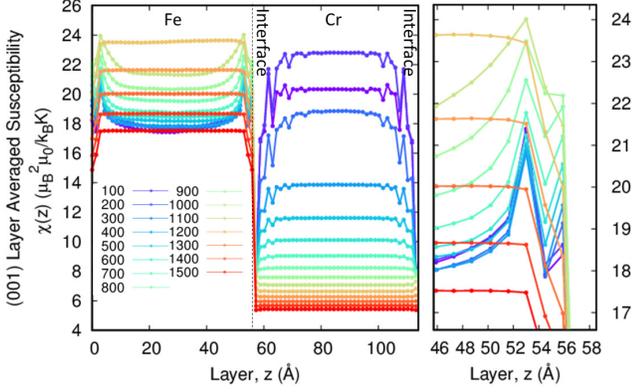
FIG. 14. Magnetic susceptibility as a function of temperature for each (001) layer in a Fe/Cr superlattice.

interfacial layers.

In Fig. 15, the autocorrelation function $c_0(z, \tau)$ shows the 1st and 3rd Fe layers (Fe(1,3)) at 100K are less correlated than the 2nd layer. This corresponds to the dip recorded in the susceptibility below 800K (see Fig. 14). Above 800K, the 2nd Fe layer becomes increasingly uncorrelated with respect to the interface layer Fe(1).

The interfacial Cr layers Cr(1), remain strongly correlated in comparison to the other Cr layers. A minimum is observed in the susceptibility at the interface for all temperatures correspondingly. At 800K, almost twice T_N, $c_1(z, \tau)$ identifies the moments in Cr(1) are still correlated to the moments of the nearest neighbouring atoms. This behaviour of the susceptibility and correlation is observed for both the (001) interface and the high order interfaces of spherical α' clusters. This identifies that studies of the simple (001) interface are good first approximations to more complex interfaces. Theoretical efforts to understand magnetic behaviour of Fe-Cr alloys would be better directed to first incorporate non-collinearity opposed to collinear models of non-ideal interfaces.

V. CONCLUSION

Spin dynamics simulations were performed to investigate the magnetic properties in $Fe_{1-x}Cr_x$ alloys with different Cr concentration and different degree of Cr precipitation. We adopted a magnetic cluster expansion Hamiltonian that allows consideration of both longitudinal and transverse fluctuations of magnetic moments within the framework of Langevin spin dynamics. We observed strong dependence of magnetic properties on the local microstructure.

Using the SPILADY code, we performed benchmarking tests against previous studies performed using Monte Carlo simulations. The two methods agree very well. Then, we compared the change of Curie temperature between disordered solutions and systems with precipitation, where in both cases the Curie temperature was
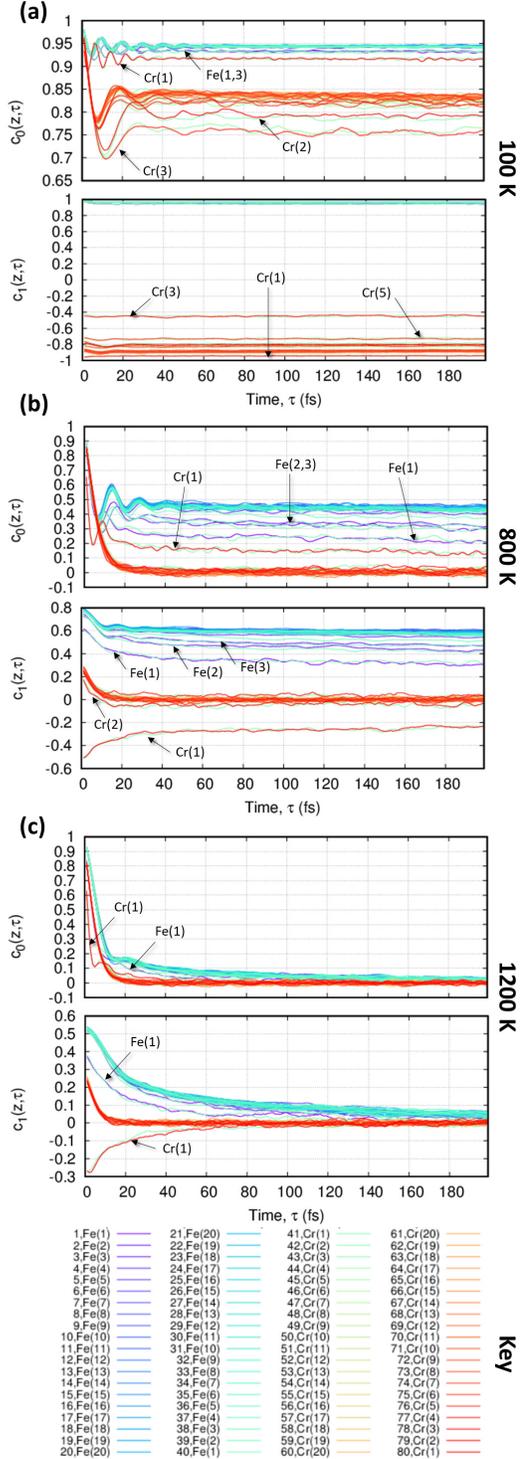
FIG. 15. Time-displaced spin-spin autocorrelation and nearest neighbour correlation functions of each (001) layer in a Fe/Cr superlattice at 100k, 800K and 1200K. Fe/Cr interface between layers 80 & 1, and 40 & 41. Curves of interest are labelled according to the atoms in the layer and their proximity to the interface. The Fe interfacial layers (1,40) are labelled as Fe(1). The next layers (2,39) are labelled Fe(2), Cr interface layers (41,80) are labelled Cr(1), and so on.

determined from the susceptibility. For the disordered solid solutions, the Curie temperature is maximum for a Cr concentration of approximately 5 at.%. On the other hand, when Cr clustering was considered, the total magnetisation for any nominal Cr concentration increased with the size of the Cr precipitate at low temperatures and was minimum for solid solutions. This means that the higher is the level of Cr precipitation, the higher is the total magnetisation.

When we observed the change in the Curie temperature for nominal concentrations of Cr with precipitates of varying size, we found a dependence upon the effective concentration. The effective concentration is the Cr concentration outside the α' cluster. The transition temperature was found to be highest for configurations with an effective α concentration of 5-6 at.%.

For a particular case of Fe-9Cr alloys, which has the same Cr concentration as EUROFER-97, the magnetisation can vary by 10% over the operational temperature ranges of the first wall of fusion power plant, for example from 600K to 800K. The change of magnetisation is due to the varying level of Cr precipitation. This potentially has significant impact on the integrity of the mechanical properties of steels, which is coupled to its magnetic properties.

Cr located at the interface were observed to have moments that remained strongly corrected over time and with respect to the neighbouring moments. The Cr moments were aligned anti-parallel to the moments of adjacent Fe atoms, reducing the susceptibility relative to Cr in the core of the cluster.

For pure Cr precipitates, the moments were identified to rotate from being anti-parallel to Fe at the interface, to being perpendicular in the centre in an antiferromagnetic configuration with respect to their nearest neighbours. Cr moments near the interface, where the noncollinear configuration was observed, were determined to be the least correlated and therefore frustrated. For impure clusters of experimentally consistent Fe concentrations (50-95%Cr), the ordered antiferromagnetic configuration in the centre of the cluster was destroyed. Instead, disordered non-collinear configurations were observed across all temperatures. A net magnetisation was still supported.

When temperature increases, the Fe moments close to the interfaces are more disorder than in the bulk. The Cr interface acts as a nucleation site with a reduced effective Curie temperature. Conversely, the Cr moments on the interface remain statistically correlated at temperatures far exceeding the Néel point.

We may understand the underlying physics through an investigation into dynamic properties which can be calculated from spin dynamics calculations in contrast to the Monte Carlo method. We studied the spin-spin autocorrelation and 1st nearest neighbour correlation functions in Cr clusters and (001) Fe-Cr superlattices. Contrary to expectation, the high index of the cluster interface does not significantly change the observed correlation of Fe and Cr across the interface with respect to the simple (001) case. Fe magnetic moments near the interface fluctuate more readily than in the bulk of the α. This resulted in enhanced susceptibility of the Fe in the interfacial layers. The dynamic properties observed for the impure clusters remained consistent with the pure clusters and (001) interface.

In future work we intend to improve on the limitations of the current model. Namely, we are developing, within a similar formalism, an Fe-Cr potential suitable for combined molecular-dynamics spin-dynamics simulations[15] which will enable the inclusion of irradiation relevant defects and coupling of magnons to lattice dynamics. The introduced anisotropies will necessarily require the inclusion of relativistic effects such as spin-orbit coupling which will break the rotational invariance of this model.

In summary, using spin dynamics we have investigated the magnetisation, the susceptibility and the Curie temperature of $Fe_{1-x}Cr_x$ alloys with different Cr concentration and different degrees of Cr precipitation. This enhances our knowledge of how magnetic properties of steels change upon ageing and under irradiation damage. This may potentially allow finding a non-invasive way of determining the level of Cr precipitation through the observation of magnetic properties of alloys.

ACKNOWLEDGMENTS

* Jacob.Chapman@ukaea.uk
[1] D. Stork, P. Agostini, J. L. Boutard, D. Buckthorpe, E. Diegele, S. L. Dudarev, C. English, G. Federici, M. R. Gilbert, S. Gonzalez, A. Ibarra, Ch. Linsmeier, A. Li. Puma, G. Marbach, P.F. Morris, L. W. Packer, B. Raj, M. Rieth, Tran M. Q., D. J. Ward, and S. J. Zinkle,

"Developing structural, high-heat flux and plasma facing materials for a near-term demo fusion power plant: The eu assessment," Journal of Nuclear Materials **455**, 277 (2014).

[2] D. Stork, P. Agostini, J.-L. Boutard, D. Buckthorpe, E. Diegele, S. L. Dudarev, C. English, G. Federici, M. R. Gilbert, S. Gonzalez, A. Ibarra, C. Linsmeier, A. Li Puma, G. Marbach, L. W. Packer, B. Raj, M. Rieth, M. Q. Tran, D. J. Ward, and S. J. Zinkle, "Materials r&d for a timely demo: Key findings and recommendations of the eu roadmap materials assessment group," Fusion Engineering and Design **89**, 1586 (2014).

[3] M. Mergia and N. Boukos, "Structural, thermal, electrical and magnetic properties of eurofer 97 steel," Journal of Nuclear Materials **373**, 1 (2008).

[4] M. Gasparotto, R. Andreani, L. V. Boccaccini, A. Cardella, G. Federici, L. Giancarli, G. Le Marois, D. Maisonnier, S. Malang, A. Moeslang, Y. Poitevin, B. van der Schaaf, and M. Victoria, "Study of in-vessel candidate materials for fusion power plants- the european materials r&d programme," Fusion Engineering and Design **66**, 129 (2003).

[5] W. Xiong, M. Selleby, Q. Chen, J. Odqvist, and Y. Du, "Phase equilibria and thermodynamic properties in the fe-cr system," Crtical Reviews in Solid State and Materials Science **35**, 125 (2010).

[6] J. O. Andersson and B. Sundman, "Thermodynamic propertis of the cr-fe system," CALPHAD **11**, 83 (1987).

[7] G. Bonny, D. Terentyev, and L. Malerba, "On the $\alpha - \alpha'$ miscibility gap of fe-cr alloys," Scripta Materialia **59**, 1193 (2008).

[8] A. W. Overhauser, "Spin density waves in an electron gas," Physical Review **128**, 1437 (1962).

[9] E. Fawcett, "Spin-density-wave antiferromagnetism in chromium," Reviews of Modern Physics **60**, 209 (1988).

[10] R. Hafner, D. Spišák, R. Lorenz, and J. Hafner, "Magnetic ground state of cr in density-functional theory," Phys. Rev. B **65**, 184432 (2002).

[11] S. K. Burke, R. Cywinski, J. R. Davis, and B. D. Rainford, "The evolution of magnetic order in crfe alloys .2. onset of ferromagnetism," Journal of Physics F: Metal Physics **13**, 451 (1983).

[12] M. Y. Lavrentiev, K. Mergia, M. Gjoka, D. Nguyen-Manh, G. Apostolopoulos, and S. L. Dudarev, "Magnetic cluster expansion simulation and experimental study of high temperature magnetic properties of fe-cr alloys," Journal of Physics: Condensed Matter **24**, 326001 (2012).

[13] D. Nguyen-Manh, M. Y. Lavrentiev, and S. L. Dudarev, "Ab initio and monte carlo modeling in fecr system: Magnetic origin of anomalous thermodynamic and kinetic properties," Computational Materials Science **44**, 1 (2010).

[14] H. Hasegawa and D. G. Pettifor, "Microscopic theory of the temperature-pressure phase diagram of iron," Physical Review Letters **50**, 130 (1983).

[15] P.-W. Ma, S. L. Dudarev, and J. S. Wróbel, "Dynamic simulation of structural phase transitions in magnetic iron," Physical Review B **96**, 094418 (2017).

[16] D. Nguyen-Manh, A. P. Horsfield, and S. L. Dudarev, "Self-interstital atom defects in bcc transition metals: Group-specific trends," Physical Review B **73**, 020101 (2006).

[17] P. M. Derlet, D. Nguyen-Manh, and S. L. Dudarev, "Multiscale modelling of crowdion and vacancy defects in body-centred-cubic transition metals," Physical Review B **76**, 054107 (2007).

[18] C. C. Fu, F. Willaime, and P. Ordejón, "Stability and mobility of mono- and di-intersistials in α-fe," Physical Review Letters **92**, 175503 (2004).

[19] P. Olsson, C. Domain, and J. Wallenius, "Ab initio study of cr interactions with point defects in bcc fe," Physical Review B **75**, 014100 (2007).

[20] D. J. Dever, "Temperature dependence of the elastic constants in α-iron single crystals: relationship to spin order and diffusion anomalies*," Journal of Applied Physics **43**, 3293 (1972).

[21] H. Hasegawa, M. W. Finnis, and D. G. Pettifor, "A calculation of elastic constants of ferromagnetic iron at finite temperatures," Journal of Physics F: Metal Physics **15**, 19 (1985).

[22] P. J. Grobner, "The 885° f (475° c) embrittlement of ferritic stainless steels," Metallurgical Transactions **4**, 251–260 (1973).

[23] S. Novy, P. Pareige, and C. Pareige, "Atomic scale analysis and phase separation understanding in a thermally aged fe-20 at.% cr alloy," Journal of Nuclear Materials **384**, 96 (2009).

[24] F. Soisson and T. Jourdan, "Radiation-accelerated precipitation in fe-cr alloys," Acta Materialia **103**, 870 (2016).

[25] E. Little and D. Stow, "Void-swelling in irons and ferritic steels: Ii. an experimental survey of materials irradiated in a fast reactor," Journal of Nuclear Materials **87**, 25 (1979).

[26] M. Bachhav, G. R. Odette, and E. A. Marquis, "Microstructural changes in a neutron irradiated fe-15at.%cr alloy," Journal of Nuclear Materials **454**, 381 (2014).

[27] T. P. C. Klaver, R. Drautz, and M. W. Finnis, "Magnetism and thermodynamics of defect-free fe-cr alloys," Physical Review B **74**, 094435 (2006).

[28] P. Olsson, I. A. Abrikosov, L. Vitos, and J. Wallenius, "Ab initio formation energies of fe-cr alloys," Journal of Nuclear Materials **321**, 84 (2003).

[29] M. Furusaka, Y. Ishikawa, S. Yamaguchi, and Y. Fujino, "Phase separation process in fe-cr alloys studied by neutron small angle scattering," Journal of the Physical Society of Japan **55**, 2253 (1986).

[30] F. Bley, "Neutron small-angle scattering study of unmixing in fecr alloys," Acta Metallurgica et Materialia **40**, 1505 (1992).

[31] S. Dubiel and J. Zukrowski, "Change of cr atoms distribution in fe85-cr15 alloy caused by 250 kev he+ ion irradiation to different doses," Journal of Alloys and Compounds **624**, 165 (2015).

[32] M. Miller, J. Hyde, M. Hetherington, A. Cerezo, G. Smith, and C. Elliott, "Spinodal decomposition in fe-cr alloys: experimental study at the atomic level and comparison with computer models i. introduction and methodology," Acta Metallurgica et Materialia **43**, 3385 (1995).

[33] A. Kuronen, S. Granroth, M. H. Heinonen, R. E. Perälä, T. Kilpi, P. Laukkanen, J. Lång, J. Dahl, M. P. J. Punkkinen, K. Kokko, M. Ropo, B. Johannson, and L. Vitos, "Segregation, precipitation, and $\alpha - \alpha'$ phase separation in fe-cr alloys," Physical Review B **92**, 214113 (2015).

[34] I. Dopico, P. Castrillo, and I. Martin-Bragado, "Quasiatomistic modeling of the microstructure evolution in binary alloys and its application to the fecr case," Acta Materialia **95**, 324 (2015).

[35] L. D. Landau and L. M. Lifshitz, "On the theory of the dispersion of magnetic permeability in ferromagnetic bodies," Physikalische Zeitschrift der Sowjetunion **8**, 153 (1935).

[36] T. L. Gilbert, "A phenomenological theory of damping in

ferromagnetic materials," IEEE Transactions on Magnetics **40**, 3443 (2004).

[37] X. Tao, D. P. Landau, T. C. Schulthess, and G. M. Stocks, "Spin waves in paramagnetic bcc iron: spin dynamics simulations," Physical Review Letters **95**, 087207 (2005).

[38] P. W. Ma, C. H. Woo, and S. L. Dudarev, "High-temperature dynamics of surface magnetism in iron thin films," Philosophical Magazine **89**, 2921 (2009).

[39] P. W. Ma and S. L. Dudarev, "Longitudinal magnetic fluctuations in langevin spin dynamics," Physical Review B **86**, 054416 (2012).

[40] P. W. Ma and S. L. Dudarev, "Parallel algorithm for spin and spin-lattice dynamics," Physical Review E **79**, 046703 (2009).

[41] J. Hubbard, "Magnetism of iron," Physical Review B **19**, 2626 (1979).

[42] W. F. Brown Jr., "Thermal fluctuations of a single-domain particle," Physical Review **130**, 1677 (1963).

[43] J. L. Garcia-Palacios and F. J. Lázaro, "Langevin-dynamics study of the dynamical properties of small magnetic particles," Physical Review B **58**, 14937 (1998).

[44] P. W. Ma, S. L. Dudarev, A. A. Semenov, and C. H. Woo, "Temperature for a dynamic spin ensemble," Physical Review E **82**, 031111 (2010).

[45] S. Chandrasekhar, "Stochastic problems in physics and astronomy," Reviews of Modern Physics **15**, 1 (1943).

[46] R. Kubo, "The fluctuation-dissipation theorem," Reports on Progress in Physics **29**, 255 (1966).

[47] P. W. Ma and S. L. Dudarev, "Langevin spin dynamics," Physical Review B **83**, 134418 (2011).

[48] P.-W. Ma, S. L. Dudarev, and C. H. Woo, "Spilady: A parallel cpu and gpu code for spinlattice magnetic molecular dynamics simulations," Computer Physics Communications **207**, 350 (2016).

[49] M. Y. Lavrentiev, S. L. Dudarev, and D. Nguyen-Manh, "Magnetic cluster expansion simulations of fecr alloys," Journal of Nuclear Materials **386**, 22 (2009).

[50] M. Y. Lavrentiev, D. Nguyen-Manh, and S. L. Dudarev, "Cluster expansion models for fe-cr alloys, the prototype materials for a fusion power plant," Computational Materials Science **49**, S199 (2010).

[51] M. Yu. Lavrentiev, D. Nguyen-Manh, and S. L. Dudarev, "Magnetic cluster expansion model for bcc-fcc transitions in fe and fe-cr alloys," Physical Review B **81**, 184202 (2010).

[52] D. Nguyen-Manh, M. Y. Lavrentiev, M. Muzyk, and S. L. Dudarev, "First-principles models for phase stability and radiation defects in structural materials for future fusion power-plant applications," Journal of Materials Science **47**, 7685 (2012).

[53] M. Yu. Lavrentiev, R. Soulairol, C. C. Fu, D. Nguyen-Manh, and S. L. Dudarev, "Noncollinear magnetism at interfaces in iron-chromium alloys: The ground states and finite-temperature configurations," Physical Review B **84**, 144203 (2011).

[54] K. Chen and D. P. Landau, "Spin-dynamics study of the critical behavior of the three-dimensional classical heisenberg ferromagnet," Physical Review B **49**, 3266 (1994).

[55] M. Yu. Lavrentiev, D. Nguyen-Manh, and S. L. Dudarev, "Magnetic cluster expansion model for chromium precipitates in fe-cr alloys," Solid State Phenomena **172**, 1002 (2011).

[56] J. Crangle and G. C. Hallam, "Magnetization of face-centred cubic and body-centred cubic iron and nickel alloys," Proceedings of the Royal Society of London Series A **272**, 119 (1963).

[57] S. Cottenier, B. De Vries, J. Meersschaut, and M. Rots, "What density-functional theory can tell us about the spin-density wave in cr," Journal of Physics: Condensed Matter **14**, 3275 (2002).

[58] W. Xiong, P. Hedström, M. Selleby, J. Odqvist, M. Thuvander, and Q. Chen, "An improved thermodynamic modeling of the fe-cr system down to zero kelvin coupled with experiments," CALPHAD **35**, 355 (2011).

[59] E. R. Reese, M. Bachhav, P. Wells, T. Yamamoto, G. R. Odette, and E. A. Marquis, "On α' precipitate composition in thermally annealed and neutron-irradiated fe- 9-18cr alloys," Journal of Nuclear Materials **500**, 192 (2018).

[60] H. Fritzsche, S. Bonn, J. Hauschild, J. Klenke, K. Prokes, and G. J. McIntyre, "Antiferromagnetic order of thin epitaxial cr layers in an fe/cr(110) multilayer," Physical Review B **65**, 144408 (2002).

[61] P.-W. Ma, C. H. Woo, and S. L. Dudarev, "Large-scale simulation of the spon-lattice dynamics in ferromagnetic iron," Physical Review B **78**, 024434 (2008).

[62] O. Tissot, C. Pareige, E. Meslin, B. Decamps, and J. Henry, "Kinetics of alpha' precipitation in an electron irradiated fe15cr alloy," Scripta Materialia **122**, 31 (2016).

[63] S. V Rogozhkin, O. A. Korchuganova, and A. A. Aleev, "Microstructural evolution of fe22%cr model alloy under thermal ageing and ion irradiation conditions studied by atom probe tomography," Inorganic Materials: Applied Research **7**, 210 (2016).

[64] Wei-Ying Chen, Yinbin Miao, Yaqiao Wu, Kun Tomchik, Carolyn A.and Mo, Jian Gan, Maria A. Okuniewski, Stuart A. Maloy, and James F. Stubbins, "Atom probe study of irradiation-enhanced alpha' precipitation in neutron-irradiated fe-cr model alloys," Journal of Nuclear Materials **462**, 242–249 (2015).